Energy 195 (2020) 117016

Contents lists available at ScienceDirect

Energy

journal homepage: www.elsevier.com/locate/energy

# Improving solar forecasting using Deep Learning and Portfolio Theory integration

Marcello Anderson F.B. Lima [a, b, *], Paulo C.M. Carvalho [a], Luis M. Fernández-Ramírez [b], Arthur P.S. Braga [a]

[a] Department of Electrical Engineering, Federal University of Ceará, Fortaleza, CE, 60455-760, Brazil
[b] Research Group in Electrical Technologies for Sustainable and Renewable Energy (PAIDI-TEP-023), Department of Electrical Engineering, University of Cadiz, EPS, Algeciras, 11202, Algeciras (Cadiz), Spain

ARTICLE INFO

*Article history:*
Received 5 August 2019
Received in revised form
13 December 2019
Accepted 20 January 2020
Available online 23 January 2020

*Keywords:*
Solar forecast
Artificial intelligence
Deep Learning
Portfolio Theory
Solar energy

ABSTRACT

Solar energy has been consolidated as one of the main renewable energy sources capable of contributing to supply global energy demand. However, the solar resource has intermittent feature in electricity production, making it difficult to manage the electrical system. Hence, we propose the application of Deep Learning (DL), one of the emerging themes in the field of Artificial Intelligence (AI), as a solar predictor. To attest its capacity, the technique is compared with other consolidated solar forecasting strategies such as Multilayer Perceptron, Radial Base Function and Support Vector Regression. Additionally, integration of AI methods in a new adaptive topology based on the Portfolio Theory (PT) is proposed hereby to improve solar forecasts. PT takes advantage of diversified forecast assets: when one of the assets shows prediction errors, these are offset by another asset. After testing with data from Spain and Brazil, results show that the Mean Absolute Percentage Error (MAPE) for predictions using DL is 6.89% and for the proposed integration (called PrevPT) is 5.36% concerning data from Spain. For the data from Brazil, MAPE for predictions using DL is 6.08% and 4.52% for PrevPT. In both cases, DL and PrevPT results are better than the other techniques being used.



## 1. Introduction

Solar energy emerges as one of the main renewable energy sources capable of contributing to supply global energy demand. Consequently, photovoltaic (PV) power has increased steadily in several countries over the past few years, thus becoming an important component for sustainable development [1]. The intermittency of PV electricity production needs to be addressed to ensure reliable and proper grid operation [2,3]. Consequently, additional costs arise for leveling out unforeseen fluctuations in electricity production [4–6]. Studies show that a 25% improvement in PV power output forecast accuracy can lead to a reduction of 1.56% (US$ 46.5 million) in the net generation cost [7].

Hence, solar forecasting is an important area with a great value to grid integration and solar power plant management [8,9]. Energy traders in international energy exchange markets, utilities/Transmission System Operators (TSOs) with their network dispatchers, and also conventional power plant operators (who provide operating reserve) require reliable information about the electricity available in the system in the next few minutes, hours, or days [10].

The performances of forecast models are affected by many elements of uncertainties, and it is not always clear how single choices

*Abbreviations:* Aerosol Optical Depth, (AOD); Artificial Intelligence, (AI); Artificial Neural Networks, (ANNs); coefficient of determination, ($R^2$); Coordination for higher Education Staff Development, (CAPES); Deep Learning, (DL); Forecast based on Portfolio Theory, (PrevPT); Institute for Energy and Transport, (IET); Long Short-Term Memory, (LSTM); Mean Absolute Error, (MAE); Mean Absolute Percentage Error, (MAPE); Mean Percentage Error, (MPE); Multilayer Perceptron, (MLP); National Council for Scientific and Technological Development, (CNPq); National Institute of Meteorology, (INMET); Photovoltaic, (PV); Photovoltaic Geographical Information System, (PVGIS); Portfolio Theory, (PT); Radial Basis Function, (RBF); Recurrent Neural Network, (RNN); Root Mean Squared Error, (RMSE); Statistical Evaluation, (SE); Support Vector Machine, (SVM); Support Vector Regression, (SVR); Transmission System Operators, (TSOs).

* Corresponding author. Department of Electrical Engineering, Federal University of Ceará, Fortaleza, CE, 60455-760, Brazil.
*E-mail addresses:* marcello@ifce.edu.br (M.A.F.B. Lima), carvalho@dee.ufc.br (P.C.M. Carvalho), luis.fernandez@uca.es (L.M. Fernández-Ramírez), arthurp@dee.ufc.br (A.P.S. Braga).

https://doi.org/10.1016/j.energy.2020.117016
0360-5442/

(e.g., the choice of a specific prediction methodology over another) or different factors (e.g., meteorological forecasting errors) contribute to the final prediction error [11].

The forecasting methods can broadly be categorized into Artificial Intelligence (AI) and conventional methods. Conventional methods include the use of stochastic time series and regression-based approaches to predict energy. The conventional methods have been widely used in previous works and are capable of yielding better results while solving linear problems, while AI methods work well with non-linear outputs [12–15], which is the case of solar irradiance [16].

In the last decades, several lines of research on AI applications have been found in the solar resource forecast sector. Among the AI methods that seek solving the problem of renewable energy forecasting, the use of Artificial Neural Networks (ANNs) must be highlighted [17]. For example, Multilayer Perceptron (MLP) to solar forecast was used in Refs. [18–20], while Radial Basis Function (RBF) was used in Refs. [21,22]. Another useful AI methodology is the Support Vector Machines (SVM) due to the strong theoretical base and high generalization capacity. Since then, the Support Vector Regression (SVR) has been developed to work with predictions [23]. The SVR use for solar forecast can be found in Refs. [24–26].

One of the emerging themes in the AI field is Deep Learning (DL), a sub-category of machine learning that relates to DL opportunities with a capacity for improvement over other AI methods. Notably, deep neural network architectures provide capabilities to learn hierarchical features from the data set while providing a more efficient representation than shallow models and improving generalization [12,27–31].

In Ref. [28], a DL method is employed for estimating the solar radiation over 30 stations in Turkey. As a conclusion, DL model yields very precise and comparable results for estimating daily global solar radiation. The short-term solar power forecast with DL is explored in Ref. [30], which proposes the use of this methodology to predict PV output 15 min earlier.

Table 1 summarizes the performance data of the techniques. It is worth mentioning that the different methodologies are used with different types of Statistical Evaluation (SE) and with different forecasting horizons. The SEs are Mean Absolute Error (MAE), Root Mean Squared Error (RMSE), Mean Absolute Percentage Error (MAPE), Mean Percentage Error (MPE) and coefficient of determination ($R^2$).

Considering the increasing use of PV plants worldwide, this paper explores the use of AI techniques, such as MLP, RBF, SVR and DL, as a solar prediction resource. These techniques were chosen after a vast bibliographical survey, which confirmed that MLP, RBF and SVR are highly consolidated, with good results in the area of solar irradiance predictability; DL is characterized as a new trend, having an ability to generalize. Hence, the four techniques can be compared and the DL improvement ability can be verified.

**Table 1**
Comparison of AI used for solar forecast.

| | TECHNIQUE | SE | RESULT SE | HORIZON | PLACE | YEAR |
|---|---|---|---|---|---|---|
| [18] | MLP | MAE | 2.75% | 24 h | ITA[a] | 2010 |
| [19] | MLP | RMSE | 32.75 W/m$^2$ | 1 h | SAU[a] | 2018 |
| [20] | MLP | MAE | 65.2 W/m$^2$ | 5 min | USA[a] | 2016 |
| [21] | RBF | MAPE | 5.44% | 1 month | USA[a] | 2015 |
| [22] | RBF | RMSE | 0.0667 W/m$^2$ | 1 day | PSE[a] | 2016 |
| [24] | SVR | MAPE | 8.94% | 1 month | DZA[a] | 2016 |
| [25] | SVR | MAE | 33.7% | 1 h | USA[a] | 2013 |
| [26] | SVR | MAE | 0.9726 | 1 month | IND[a] | 2017 |
| [28] | DL | $R^2$ | 0.98 | 1 day | TUR[a] | 2018 |
| [30] | DL | RMSE | 2.1 kW | 15 min | USA[a] | 2019 |

[a] ITA: Italy; SAU: Saudi Arabia; USA: United States; PSE: Palestinian Territories; IND: India; DZA: Algeria; TUR: Turkey.

In addition to the application and comparison of the above-mentioned solar forecasting techniques, a new strategy of integrating these techniques is herein proposed in order to reduce forecasting errors and to compare and prove the improvement of forecasting results of techniques working together. The proposed integration, herein called Forecast based on Portfolio Theory (PrevPT), uses as fundament the Portfolio Theory (PT). PT has the ultimate goal of providing a method to define the penetration percentage of each asset in order to increase financial returns. Hence, PT proposes to achieve the same profits, or greater profits, by combining investment assets [4,32].

The proposed PrevPT develops a new AI integration topology based on adaptive structural use and also adaptive weights of the MLP, RBF, SVR and DL, integrating them through the interconnection points defined by this adaptation in order to obtain smaller forecast errors. With the diversification of forecast assets, it is expected that when one of the assets obtains negative signal prediction errors, another, or other assets, complement with a countersign value, so that there is a complete or partial error cancellation.

Over the past few decades, several research lines have been found about PT applications in the energy planning sector as well as the design of energy security policies and analysis of investment in renewable power generation [4,33–38], although, to the best of the authors' knowledge, no research about the use of PT for the integration of different forecasting techniques of intermittent energy resources was found. PrevPT, as a strategy developed herein to improve the predictability of intermittent energy resources with AI integration, is an innovative contribution.

PrevPT is proposed as a contribution with beneficial characteristics in comparison to other integration techniques, such as: simple implementation and low computational cost due to the use of known statistical tools, which are improvements with regard to techniques such as Bayesian Model Averaging and Decision Trees, which use their own complex equations [39]; ability to improve the results in relation to isolated techniques, besides applying different weights according to asset performance, thus enhancing the Equal Weights technique [40].

As a methodology application, solar irradiation data and ambient temperature from Fortaleza/Brazil (latitude: −03°43′, longitude: −38°32′, elevation: 21 m (68.90 ft)) and from Algeciras/Spain (latitude: 36°13′, longitude: −5°45', elevation: 13 m (42.65 ft)) are used.

## 2. Methodology

### 2.1. Data collection

To better understand solar resource behavior, solar irradiance and ambient temperature data from Algeciras, Spain and from Fortaleza, Brazil are considered. Irradiance and ambient temperature data from Spain is obtained using the Photovoltaic Geographical Information System (PVGIS) of the European Commission/Institute for Energy and Transport (IET). Solar irradiance and temperature data are collected and stored in electronic spreadsheets in 1-h intervals. Data collection period is from January 2007 to December 2016, totaling ten years of collection and resulting in 87,672 solar irradiance and ambient temperature measurements. For the AI training, 8 years of all collected data are used (2921 days; 70,128 measurements).

In Brazil, irradiance data is measured by the Federal University of Ceará (UFC) using a pyranometer (NRG Systems, LI-200SZ); ambient temperature data is obtained using a temperature sensor

(NRG Systems, # 110S), with a precision of ±1.11 °C and operating between −40 °C and 52.5 °C. Solar irradiance and temperature data are collected and stored in electronic spreadsheets in 10-min intervals; stored values are obtained by calculating arithmetic averages of data processed every 2 s. Data collection period is from May 2003 to April 2005, totaling two years of collection and resulting in 61,404 solar irradiance and ambient temperature measurements, recorded daily from 05:00 a.m. to 06:00 p.m. For the AI training, 70% of all collected data are used (512 days; 43,008 measurements).

### 2.2. Data processing

Data were processed in order to identify outliers, which were determined using ambient temperature and solar irradiance at the study site. The data used for the determination of the upper and lower limits in Fortaleza and in Algeciras came from the National Institute of Meteorology (INMET) and from the European Commission/IET, respectively. In all cases, outliers were subsequently replaced by the values of previous measurements showing no system failure.

### 2.3. MLP

MLP consists of a neural network organized in layers. Input layer refers to the data; output layer; and hidden layers (intermediate) are made up of neurons capable of processing data, resulting in outputs assigned through inputs excitations and respective weights. Fig. 1 shows a multi-layered network having three neurons in the input layer, two neurons in the hidden layer and one in the output layer.

$X_0$, $X_1$ and $X_2$ represent the input variables, $w_i$ is weight between layers and y is the MLP output. The algorithm used for ANN training is Backpropagation, a generalization of the Widrow & Hoff delta rule for Adaline training. The name "backpropagation" is used because error propagation occurs in the reverse direction to the input signal. Widrow & Hoff Delta Rule generalization is used to adjust the weights and bias of the MLP network in order to minimize the error between the network output and the desired output [23].

Among the activation functions of the neurons, the activation function used for both the hidden neurons layer and the output layer was the logistic sigmoid, which generates values ranging 0 to 1. Equation (1) represents the function and its derivative, where $y_j$ is the neuron output of the neuron and $u_j$ is the weighted sum of all inputs.

$$y_j = \frac{1}{1+\exp(-u_j)} \tag{1}$$

The weights update of both the hidden and the output layer is given by equations (2) and (3), where $w$ is the weight, $\alpha$ is the learning rate arbitrated by the programmer, $\delta$ is the sensitivity and $b$ is the bias.

$$w_{(t+1)} = w_{(t)} + \alpha\delta y_{i(t)} \tag{2}$$

$$b_{(t+1)} = b_{(t)} - \alpha\delta \tag{3}$$

### 2.4. RBF

RBF is an ANN with multiple layers, each with different activities. The input layer is the ANN connection point with the data environment to be processed. The second layer is a single layer, which applies a nonlinear transformation of the input space to a representation in the space generated by the neuron activations of the hidden layer. The third layer is the ANN output.

RBF ANN structure is illustrated in Fig. 2, where $X_0$, $X_1$ and $X_2$ represent the input variables, $\phi_1$ and $\phi_2$ are the intermediate neurons, where each neuron has a radial base function, $y$ is the neuron that represents the ANN output, and $w_i$ is the weight of the connections between intermediate and output layer.

This ANN uses activation functions with local receptive fields, as previously mentioned [21]. Equations (4) and (5) were considered using the Gaussian function, where $\phi$ is the output of each neuron of the hidden layer, $r$ is the difference between the input x and the center t, and $\sigma$ is the measure of the curve scattering.

$$\phi = \exp\left(-\frac{r^2}{2\sigma^2}\right) \tag{4}$$

$$r = ||x - t|| \tag{5}$$

RBF output is formed by a single linear neuron, where the sum of each output of the hidden layer neurons is weighted by their respective weights, according to (6), where $y$ is the output of ANN and $w$ the weight.

$$y = \sum w_j \phi_j \tag{6}$$

### 2.5. SVR

The support vector machine (SVM) was developed by Vapnik in 1995 to solve the classification problem. This method was extended to the regression domain and prediction problems, thus being called SVR [23].

SVR structure is illustrated in Fig. 3, where $X_0$, $X_1$ and $X_2$ represent the input variables, $K_{(x,\,x1)}$ and $K_{(x,\,x2)}$ are the intermediate neurons, $y$ is the neuron that represents the AI output, and the parameters $w_i$ are the weights of the connections between intermediate and output layer.

The kernel $K_{(x,\,x')}$, is found through equation (7). Where, x is the input vector and $\sigma$ is the kernel parameter which defines the structure of the high dimensional feature space.

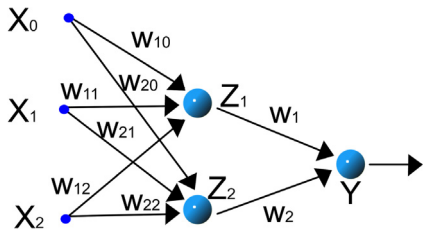


**Fig. 1.** MLP structure.

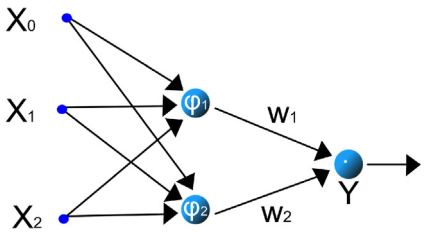


**Fig. 2.** RBF structure.

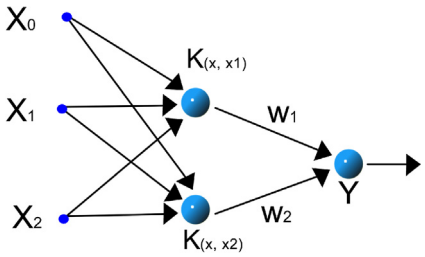


**Fig. 3.** SVR structure.

$$K_{(x,x')} = \exp\left(-\frac{||x - x'||^2}{2\sigma^2}\right) \quad (7)$$

SVR output is formed by a single linear neuron, where the sum of each output of the hidden layer neurons is weighted by their respective weights, according to (8), where $y$ is the output of AI and $w$ the weight.

$$y = \sum w_j . K_{(x,x')j} \quad (8)$$

### 2.6. DL

DL algorithms are machine learning methods based on distributed representations. DL attempts to learn high-level features in data by using structures made up of multiple non-linear transformations [41]. For producing solar irradiance predictions, a Long Short-Term Memory (LSTM) is used [42], which is an artificial Recurrent Neural Network (RNN) architecture in the field of DL [43]. LSTMs have an advantage over conventional ANNs because of their property of selectively remembering patterns for long durations of time, as shown in the process of the LSTM model with five layers (input layer, hidden layer, context layer, forget layer, and output layer) in Fig. 4.

$X_t$ is the input of the LSTM; in the case of solar predictability, a window of historical data of solar irradiance and ambient temperature collected at the mentioned sites, σ is a sigmoidal function, ϕ is a hyperbolic function and the subscripts $(f, i, z, o)$ represent the forget layer, the output and the state input for the next stage. $Y_t$ is the output of the LSTM, which is represented by the equation (9), where $f$ is the activation function for each stage, $W$ refers to the weights of each stage $(W_f,\ W_i,\ W_z,\ W_0)$, $U$ also the weight of each stage $(U_f,\ U_i,\ U_z,\ U_0)$ and $b$ is the bias of each stage $(b_f,\ b_i,\ b_z,\ b_0)$.

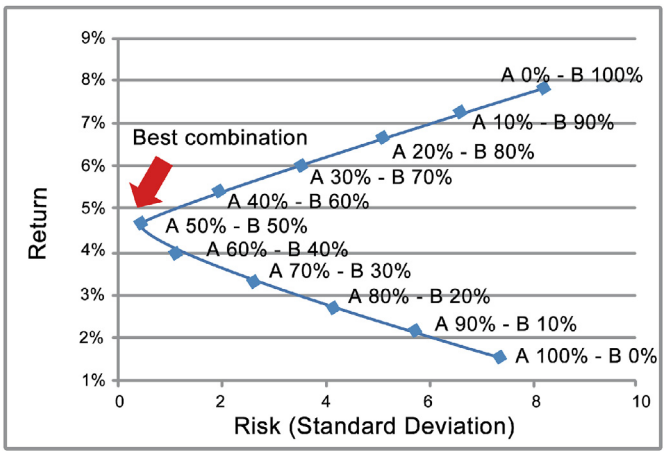


**Fig. 5.** Efficient frontier.

$$Y_t = f(W.h_{t-1} + U.x_t + b) \quad (9)$$

The context layer $C_t$, has its output defined by equation (10) and the output of the hidden layer $h_t$, in (11).

$$c_t = f_t.c_{t-1} + i_t.z_t \quad (10)$$

$$h_t = o_t.\phi c_t \quad (11)$$

### 2.7. Fine adjustments

Fine adjustments were developed using the increment method to define the amount of AIs inputs and hidden processing units. Hence, with each increase in the number of entries, starting from 1, the AIs were retrained. The algorithm found the validation value for current situation and stored it in a vector. After the limit of increments was reached, the refiner developed found the optimal

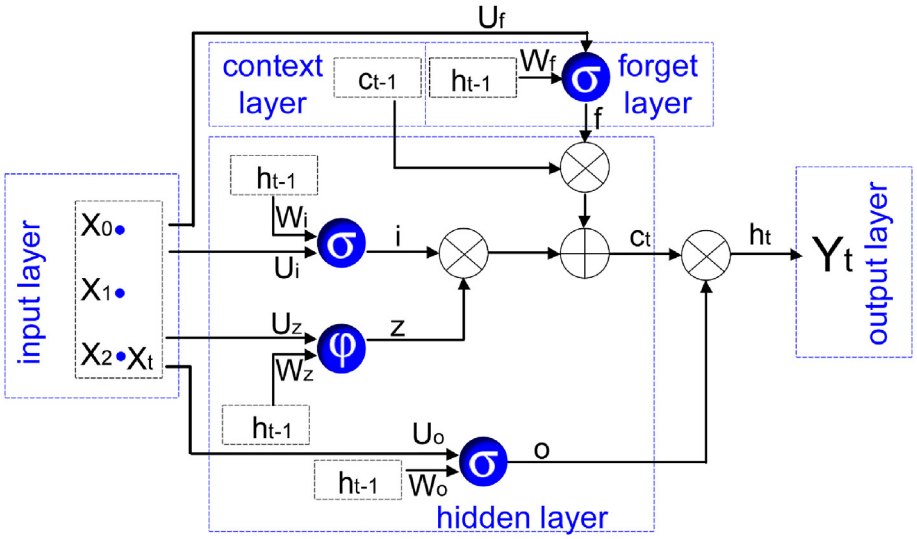


**Fig. 4.** Process of the LSTM model with five layers.

point, i.e., the ideal amount of system entries that gives a smaller amount of errors. This methodology is repeated for the four AIs used in the present research for solar forecasting.

The algorithm is also applied for the refinement of the number of hidden layer processing units of MLP, RBF and DL. For SVR, the training structure itself is capable of defining the amount of support vectors in the hidden layer. The AI refinement algorithm is defined in (12).

$$A_o = \min_{j=1}^{m} \left[ \left( \left( \sum_{i=1}^{n} \left| \frac{(D_{p(i)} - D_{o(i)}).100}{D_{o(i)}} \right| \right) . \frac{1}{n} \right)_j \right] \quad (12)$$

Where $D_p$ is the predicted data, $D_o$ is the observed data, n the total amount of forecasts and m is the increment limit.

### 2.8. Prediction errors

To validate the AI results, solar irradiance and temperature data reserved for the test period are used to characterize the operation of forecasting techniques and their respective solar resource forecasting capabilities. By comparing AI forecasting results and data collected in the same period, the percentage of errors can be calculated. Solar prediction errors can be found at different times of day, i.e., at different levels of solar resource availability [4].

Hence, to adjust forecast errors and, at the same time, take into account the amplitude of solar resource availability, a filter called Impact Factor is applied, according to (13) and (14). $D_p$ is the predicted data, $D_m$ is the measured data, $M_r$ represents the highest value of the resource under investigation in the period and $F_i$ is the Factor Impact [4].

$$E_{pp} = \frac{(D_p - D_m).100}{D_m} F_i \quad (13)$$

$$F_i = \frac{D_m}{M_r} \quad (14)$$

### 2.9. PrevPT

Asset diversification of an investment, when measured by the correlation coefficient, can be found by using the (15), in which $p_{xy}$ is the correlation coefficient between the assets $x$ and $y$; $Cov(y,x)$ is the covariance between $x$ and $y$; $\sigma_x$ is the standard deviation of asset $x$; and $\sigma_y$ is the standard deviation of asset $y$.

$$p_{xy} = \frac{Cov(y,x)}{\sigma_x \cdot \sigma_y} \quad (15)$$

Covariance between $x$ and $y$ is determined by (16), in which $xi$ represents the asset values of $x$; $\bar{x}$ is the average value of asset $x$; $yi$ is the asset values of $y$; $\bar{y}$ is the average value of asset $y$; and $n$ is the amount of asset values.

$$Cov(y,x) = \frac{\sum_{i=1}^{n} \text{Unsupported} \quad (xi - \bar{x}).(yi - \bar{y})}{n} \quad (16)$$

Portfolio risk can be determined by a statistical tool called standard deviation, which reveals the probability of a given result. In order to define the percentage of each asset and thereby reduce forecasting errors, it is necessary to set up an Efficient Frontier chart. Those boundaries are lines formed by the proportion of different assets in a portfolio, thus representing graphically how a particular return can promote the lowest possible risk [4]. Fig. 5 shows the hypothetical situation of a diversified application using assets A and B as an example of the risk-return analysis curve (Efficient Frontier).

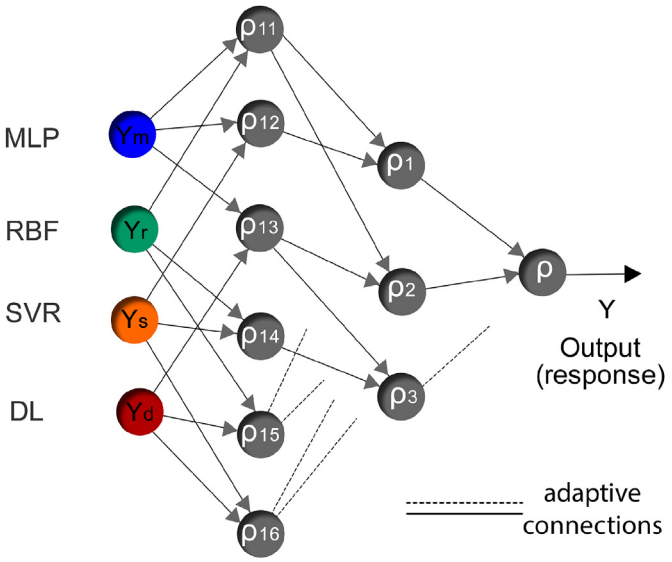


**Fig. 6.** PrevPT structure.

PrevPT structure is shown in Fig. 6, showing the use of the MLP, RBF, SVR and DL structures and their integration through the connection points ($p_{11}$ to $p_{16}$). In a later layer, PrevPT creates all possible combinations between the connections of the previous layer, and in its self-adaptive structure characteristic, it chooses the three best combinations from the measurement of their respective MAPEs. In this step, the combinations are called $p_1$ to $p_3$. In the PrevPT output, ie $p$, the two best ones between $p_1$ to $p_3$ are chosen to format a response of the algorithm.

After the training, in the testing stage, PrevPT structure can be simplified according to Fig. 7 by assigning final weights for the interconnection of forecasting techniques.

According to the topology, PrevPT develops parallel integration of techniques. The data processing steps performed by PrevPT are presented in Fig. 8 and are divided into: data collection, application of predictability techniques (MLP, RBF, SVM and DL), calculation and analysis of prediction errors, design of efficient frontiers for integration (several layers); presentation of results.

The weights are defined based on data collected from each study site, as well as the ability of each technique to accurately predict the solar availability value of each site. Hence, to obtain the ideal combination and define the percentage of each forecasting asset, the technique is simply retrained with data from the new location

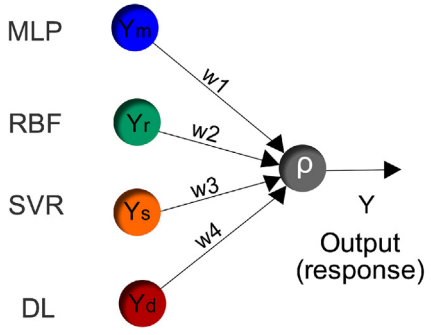


**Fig. 7.** PrevPT simplified structure.

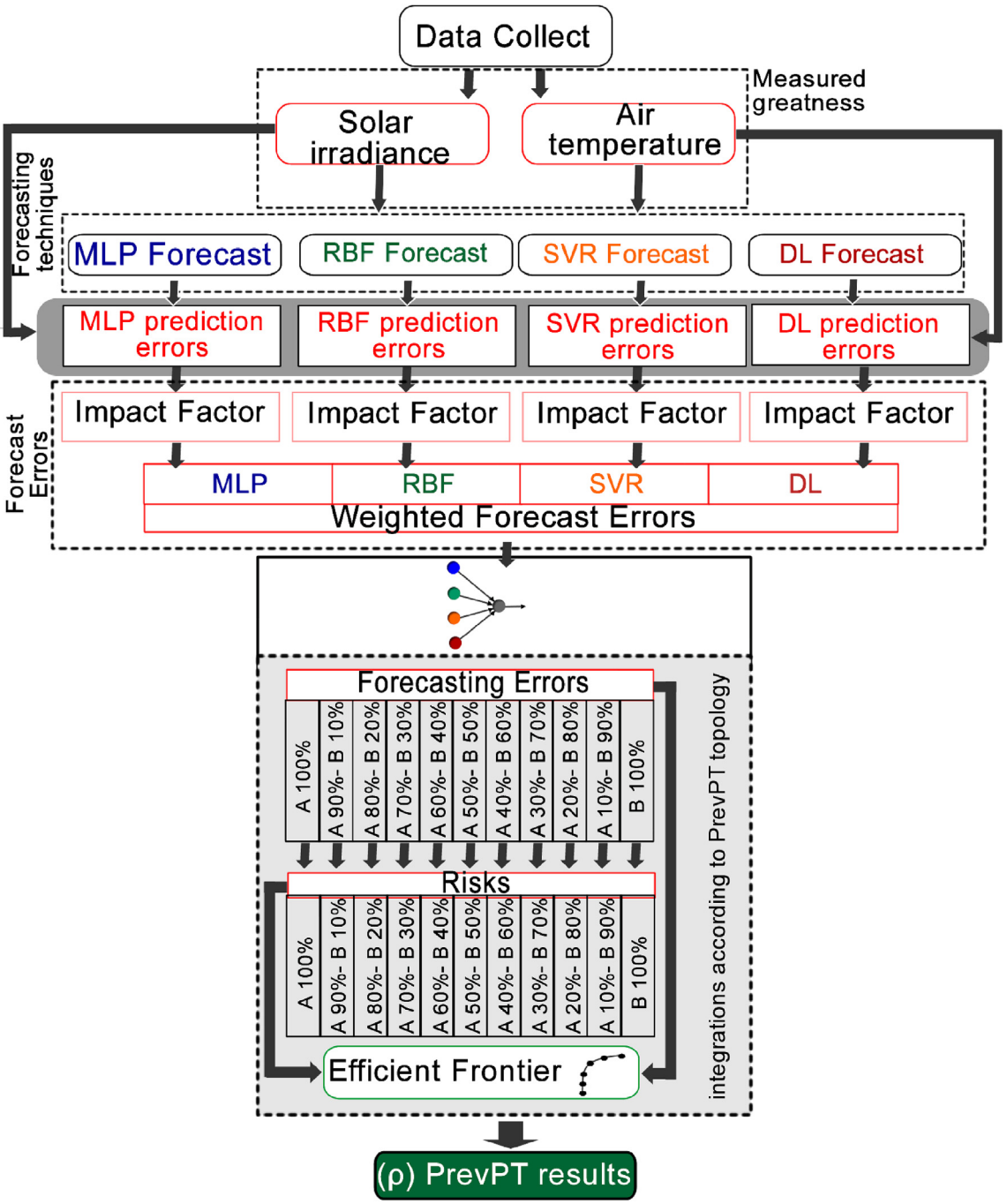


**Fig. 8.** PrevPT data processing steps.

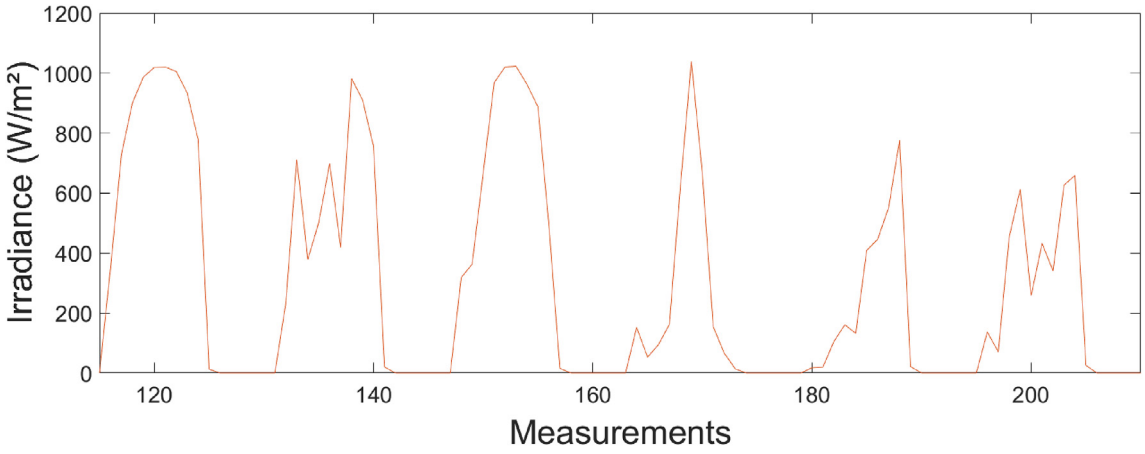


**Fig. 9.** Solar irradiance data in January 2007, Algeciras, Spain.

to obtain the final fixed weight.

Finally, it is worth noting that the proposed methodology can be applied to any technology that requires solar resource forecasting to define the energy available in the system. For example, grid-connected photovoltaic plants, off-grid photovoltaic powered water pumping systems, concentrated solar power units, amongst others.

## 3. Results and discussions

### 3.1. Characteristics of the collected data

10 years of collected data were used in Spain. They are consecutive data and all weather conditions in the period (including rainy and cloudy days) are considered. It is noteworthy that, at the place of measurement of the Spanish data, it does not snow, and this issue was not observed, but all four year seasons, different days, days with more or less solar availability are observed. For Brazil, consecutive data from 2 years of collected data were used, also experiencing all the climatic conditions in the period. Therefore, the techniques were evaluated with different climates and weather conditions in Spain and Brazil in order to conclude the best technique under two different climatic conditions, with different solar resource availability and different locations.

During data collection, Spain showed an average daily solar irradiation of 5.32 kW h/m$^2$, variance of 941.89 kW/m$^2$ and standard deviation of 970.51 W/m$^2$, while in Brazil the average daily irradiation was 6.73 kW h/m$^2$, a variance of 101.33 kW/m$^2$ and standard deviation of 318.33 W/m$^2$.

### 3.2. Forecasting errors in Spain

Fig. 9 shows 6 days of solar irradiance in Spain in January 2007 to exemplify sudden fluctuations during measurements as a consequence of cloud cover.

The predictive errors of the Spanish solar resource were found using PrevPT. Fig. 10 shows the prediction error behavior for a 300 small sample window extracted from the MLP, RBF, SVR and DL forecasts (January 1$^{ST}$, 2015 to January 19$^{TH}$, 2015). It can be seen in Fig. 10 that the forecasting errors of each technique were sometimes of opposite signal to the other techniques, which highlights that this characteristic is beneficial for the integration of the forecasting assets with the PrevPT, since theory achieves error cancellation through the ideal combination of predictors. It can also be observed that, when one of the forecasting techniques had a high error rate, the other errors were significantly lower. As an example of this, instant 50 of the displayed window, where MLP had a 42.46% error, while RBF had a 3.83% error, SVR with 3.87% and Deep Learning −0.76% error.

The highest solar irradiance value predicted by MLP is 1075.5 W/

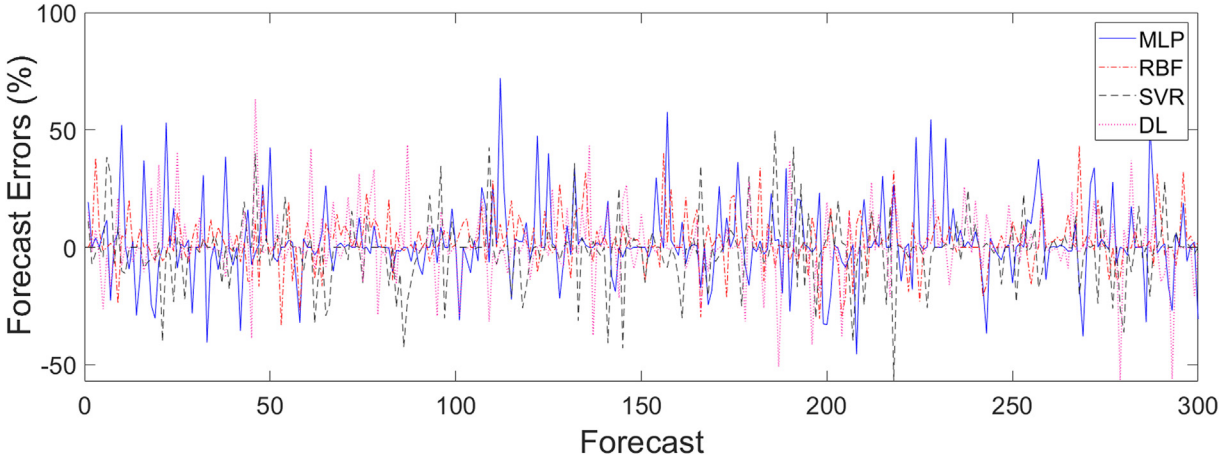


**Fig. 10.** Forecast errors in January 2015, Algeciras, Spain.

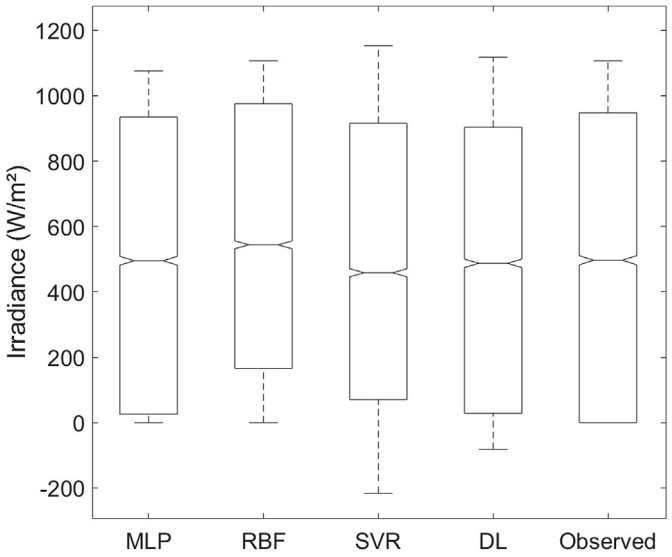


**Fig. 11.** Observed and forecast data boxplot for Algeciras, Spain.

$m^2$; the highest value predicted by RBF is 1106.8 W/$m^2$; the highest value predicted by SVR is 1171.8 W/$m^2$; and the highest value predicted by DL is 1117.3 W/$m^2$. The highest irradiance value collected during the period was 1106.83 W/$m^2$. For the MLP Backpropagation, 32.76% of the forecasts underestimates solar energy availability, 25.03% produces error 0 (zero) and 42.21% overestimates solar resource. The highest negative error is −69.52%, while the highest positive error is 81.77%; 71.29% of the predictions show forecasting errors between −10% and 10%. Average forecasting error is 1.29% and MAPE for this ANN is 8.06%.

For RBF, 21.13% of the forecasts underestimates solar energy availability, 25.02% produces error 0 (zero) and 53.85% of the predictions overestimates solar resource. The highest negative error is −57.45%, while the highest positive one is 56.96%. 73.27% of the predictions show forecasting errors between −10% and 10%. Average prediction error is 2.76% and MAPE for this ANN is 7.16%.

For SVR, 41.78% of the forecasts underestimates solar energy availability, 25.01% produces error 0 (zero) and 33.21% of the predictions overestimates solar resource. The highest negative error is −85.49%, while the highest positive one is 75.77%. 73.71% of the predictions show forecasting errors between −10% and 10%. Average prediction error is −0.89% and MAPE for this ANN is 8.34%.

For DL, 44.26% of the forecasts underestimate solar energy availability, 25.02% produces error 0 (zero) and 30.72% of the predictions overestimate solar resource. The highest negative error is −63.52%, while the highest positive one is 72.93%. 75.87% of the predictions show forecasting errors between −10% and 10%. Average prediction error is 0.36% and MAPE for this ANN is 6.89%. The MAPE presented by the four prediction techniques represents the superiority of DL compared to other solar resource forecasting strategies. Fig. 11 shows the boxplot to represent the variation of observed and forecast data by the proposed AI techniques.

The interquartile range limits (50% of the data presented) was 27.07 W/$m^2$ to 934.47 W/$m^2$ for MLP; 165.86 W/$m^2$ to 975.16 W/$m^2$ for RBF; 70.5 W/$m^2$ to 915.45 W/$m^2$ for SVR; 28.76 W/$m^2$ to 903.17 W/$m^2$ for DL; and 0 W/$m^2$ to 947.5 W/$m^2$ for the data collected in the trial period. As can be seen, the best results were achieved by DL. SVR also obtained good results, although with some negative values, which is impossible to happen.

### 3.3. Integration of techniques in Spain

For designing the Efficient Frontier, a total of 21 combinations of each connection is used according to the proposed topology, each with different weighting, seeking the lowest risk of forecast errors. The combinations are made from 100% of asset A and 0% of asset B up to 0% of asset A and 100% of asset B. Changes in the percentages with steps are made every 5%, which generates the 21 combinations above. To illustrate this, in connection $p_{11}$, which combines RBF and DL for example: 21 combinations are assembled with different percentage levels of each AI used, ranging from 100% forecast RBF usage and 0% DL usage, later 95% RBF and 5% DL, until 0% RBF forecast usage and 100% DL usage is achieved. The risk and the prediction error of the combination for efficient frontier plotting are found at each combination. After the integrations, predictability error risks and predictability errors for each combination are found. Fig. 12, Fig. 13 and Fig. 14 show the Efficient Frontiers of PrevPT for the Spanish data.

The first layer of PrevPT is defined with connection $p11$ (55% RBF - 45% DL), connection $p12$ (45% MLP − 55% DL) and connection $p13$ (40% MLP − 60% RBF). The second layer is defined with connection $p$ 1 (60%− $p11$ 40% $p$ 12) and connection $p$ 2 (55%− $p11$ 45% $p13$). PrevPT output is defined as 50% $p$ 1 and 50% $p2$.

Efficient Frontier results show that the optimal portfolio, i. e., the combination with best predictability results, is 18% MLP, 45.12% RBF, 0% SVR and 36.88% DL. This result is achieved by using the lowest standard deviation found, i. e., the combination, for the generated portfolio, with results that have the least chance of showing erratic behavior compared to other study data. PrevPT, in its characteristic of self-adaptive structure, found the best

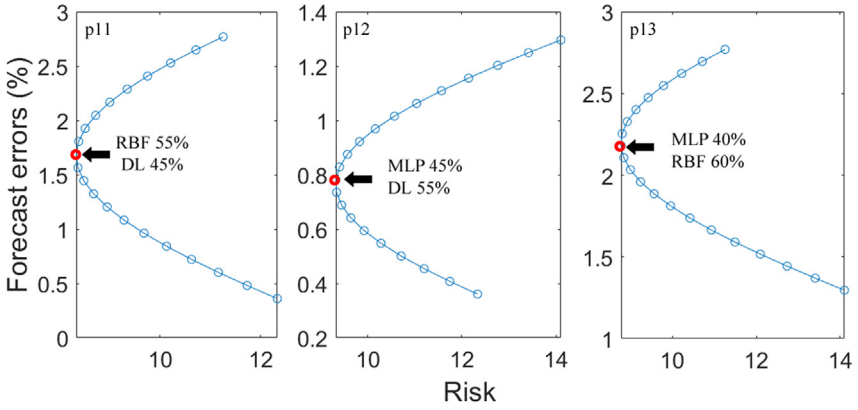


**Fig. 12.** Developed efficient frontiers (first layer).

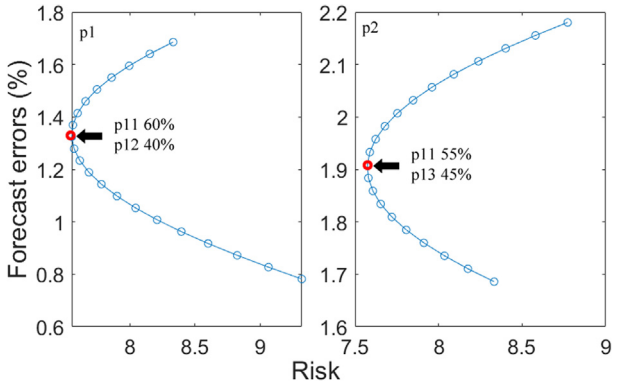


**Fig. 13.** Developed efficient frontiers (second layer).

combination that can be seen in Fig. 15 (a) in its complete structure and (b) in its simplified form mathematically.

The comparison between the distribution of prediction errors is shown in Fig. 16.

For PrevPT, 39.76% of the forecasts underestimate and 58.84% overestimates solar resource. The highest negative error is −34.47%, while the highest positive one is 38.16%. 83.42% of the predictions show forecasting errors between −10% and 10%. Average forecasting error is 1.61% and MAPE is 5.36%, which defines integration methodology as an improvement of individual AI results, since MLP MAPE is 8.06%, RBF MAPE is 7.16%, SVR MAPE is 8.34% and DL MAPE is 6.69%. Table 2 compares individual AI results, partial and final integrations made by PrevPT for the Spanish data. The comparison uses the same database, horizons and forecast period, in order to generate an SE of the forecasting techniques using the MAPE, MPE and Range −10 (%) to 10 (%).

In the city of Algeciras, the climate is well defined with four seasons (winter, spring, summer, autumn). For this reason, the data collected for these four sessions were separated during the test period to prove the applicability of the techniques used here under different climatic conditions. Table 3 compares the MAPEs values obtained for all sessions. MAPEs values of the different techniques (AIs and PrevPT) are very similar for all cases.

Fig. 17 presents the Boxplot of the forecasting techniques for the four situations. The results show that the behavior of the techniques is very similar for all sessions with different solar availability. This characteristic can be observed comparing the DL interquartile range limits: 2.79%–0.98% for winter, −2.66%–0.78% for spring, −2.96%–0.84% for summer and −3.11%–0.63% for autumn.

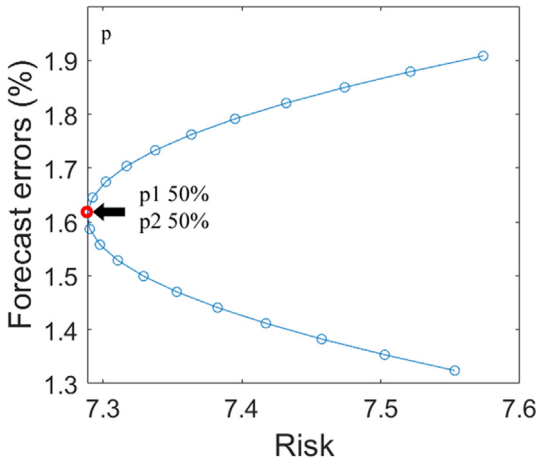


**Fig. 14.** Developed efficient frontiers (output).

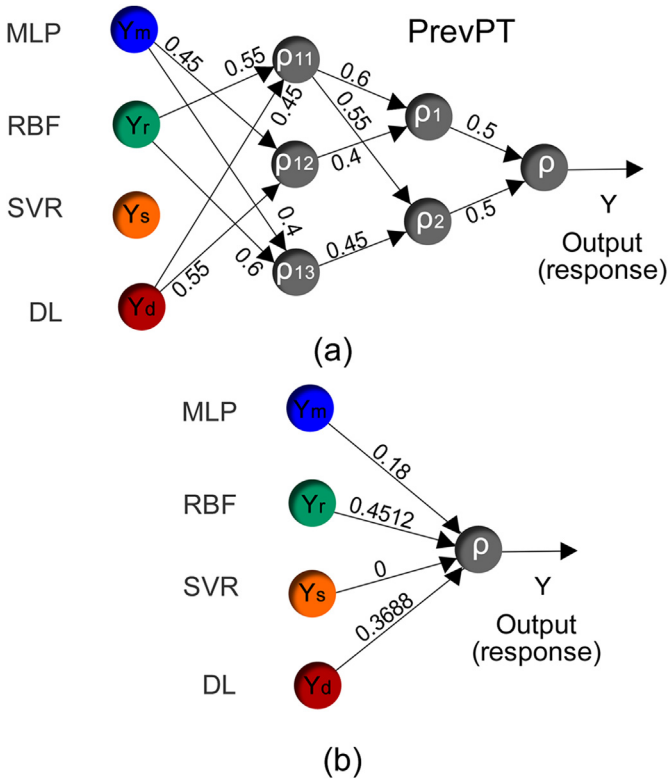


**Fig. 15.** Final weights and structure PrevPT Spain.

### 3.4. Forecasting errors in Brazil

Fig. 18 shows the prediction error behavior for a 500 small sample window extracted from the forecasts made with MLP, RBF, SVR and DL (September 23$^{TH}$, 2004 to September 30$^{TH}$, 2004).

The highest solar irradiance value foreseen by MLP is 1011.9 W/m2, the highest value predicted by RBF is 1203 W/m$^2$, the highest value predicted by SVR is 1016.2 W/m$^2$ and the highest value predicted by DL is 1203 W/m2. The highest measured irradiance is 1203 W/m$^2$.

For MLP, 28.57% of the forecasts underestimate solar potential, 7.06% produce error 0 (zero) and 64.37% overestimate solar resource. The highest negative error is −43.19%, while the highest positive one is 72.4%. 70.48% of the predictions show forecasting errors between −10% and 10%. Average forecasting error is 6.01% and MAPE for this ANN is 8.53%.

For RBF, 81.73% of the forecasts underestimate solar energy availability, 7.02% produce error 0 (zero) and 11.25% of the predictions overestimate solar resource. The highest negative error is −42.58%, while the highest positive one is 36.77%. 75.73% of the predictions show forecasting errors between −10% and 10%. Average prediction error is −5.27% and MAPE for this ANN is 6.32%.

For SVR, 36.6% of the forecasts underestimate solar energy availability, 7.04% produce error 0 (zero) and 56.36% of the predictions overestimate solar resource. The highest negative error is −63.49%, while the highest positive one is 58.81%. 72.32% of the predictions show forecasting errors between −10% and 10%. Average prediction error is 0.35% and MAPE for this ANN is 8%.

For DL, 47.88% of the forecasts underestimates solar energy availability, 7.04% produces error 0 (zero) and 45.08% of the

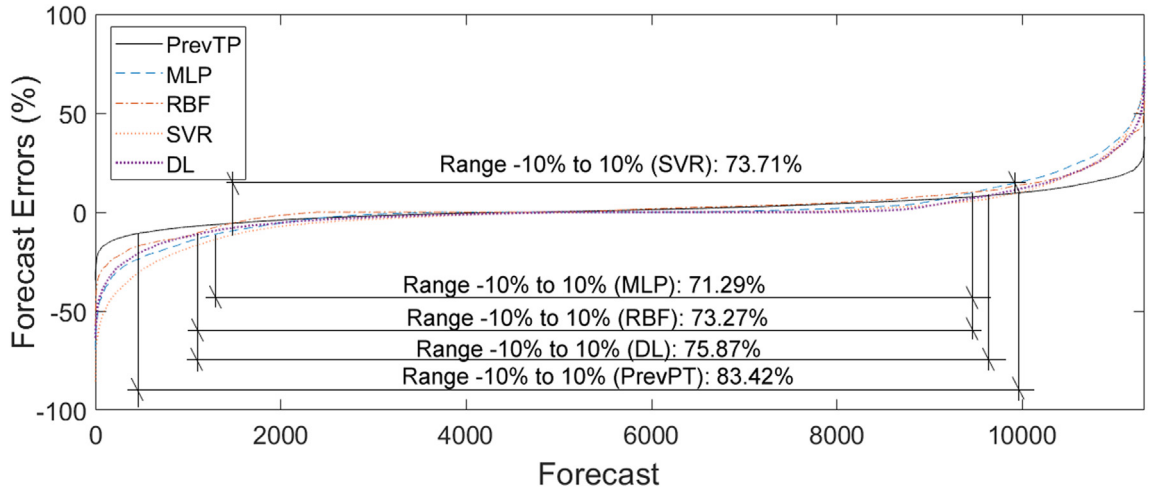


**Fig. 16.** Forecasting error distributions for the Spanish data.

**Table 2**
Comparison of the forecasting results for the Spanish data.

| | MAPE (%) | MPE (%) | Range −10 (%) to 10 (%) |
|---|---|---|---|
| MLP | 8.06 | 1.29 | 71.29 |
| RBF | 7.16 | 2.76 | 73.27 |
| SVR | 8.34 | −0.89 | 73.71 |
| DL | 6.89 | 0.36 | 75.87 |
| MLP/RBF | 6.28 | 2.18 | 78.09 |
| MLP/SVR | 6.88 | 0.31 | 73.99 |
| RBF/SVR | 6.29 | 1.48 | 77.33 |
| MLP/RBF/SVR | 5.66 | 1.7 | 82.02 |
| MLP/RBF/SVR/DL | 5.36 | 1.61 | 83.42 |

**Table 3**
MAPE for the four sessions in Spain.

| | Winter | Spring | Summer | Autumn |
|---|---|---|---|---|
| MLP | 8.16% | 8.14% | 7.8% | 8.17% |
| RBF | 7.22% | 7.13% | 7.23% | 7.07% |
| SVR | 8.12% | 8.5% | 8.07% | 8.64% |
| DL | 7.19% | 6.67% | 6.89% | 6.81% |
| PrevPT | 5.54% | 5.25% | 5.37% | 5.27% |

predictions overestimates solar resource. The highest negative error is −62.93%, while the highest positive one is 51.34%. 78.68% of the predictions show forecasting errors between −10% and 10%. Average prediction error is 0.06% and MAPE for this ANN is 6.08%. Fig. 19 shows the boxplot to represent the variation of observed and forecast data by the proposed AIs.

The interquartile range limits was 124.6 W/m$^2$ to 1011.89 W/m$^2$ for MLP, 30.19 W/m$^2$ to 618.14 W/m$^2$ for RBF, 141.76 W/m$^2$ to 678.23 W/m$^2$ for SVR, 107.66 W/m$^2$ to 679.25 W/m$^2$ for DL and 66.04 W/m$^2$ to 711 W/m$^2$ for the data collected in the trial period. The best results were achieved by DL.

### 3.5. Integration of techniques in Brazil

After the integrations, predictability error risks and predictability errors for each combination are found. Fig. 20, Fig. 21 and Fig. 22 show the Efficient Frontiers of PrevPT for the data from Brazil.

The first layer of PrevPT is defined with connection $p11$ (25% MLP - 75% RBF), connection $p12$ (65% RBF − 35% DL) and connection

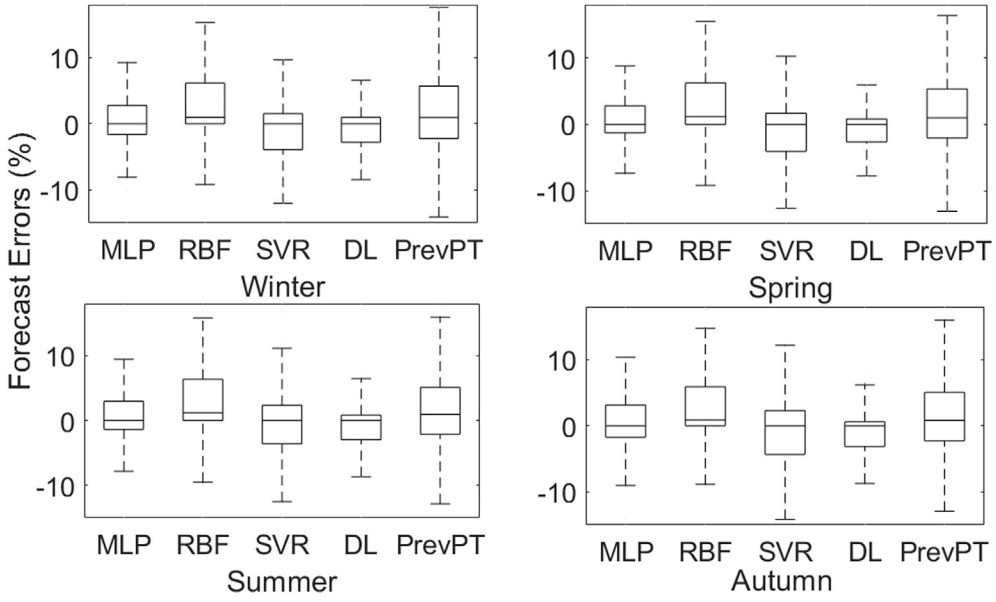


**Fig. 17.** Boxplot for the four sessions in Spain.

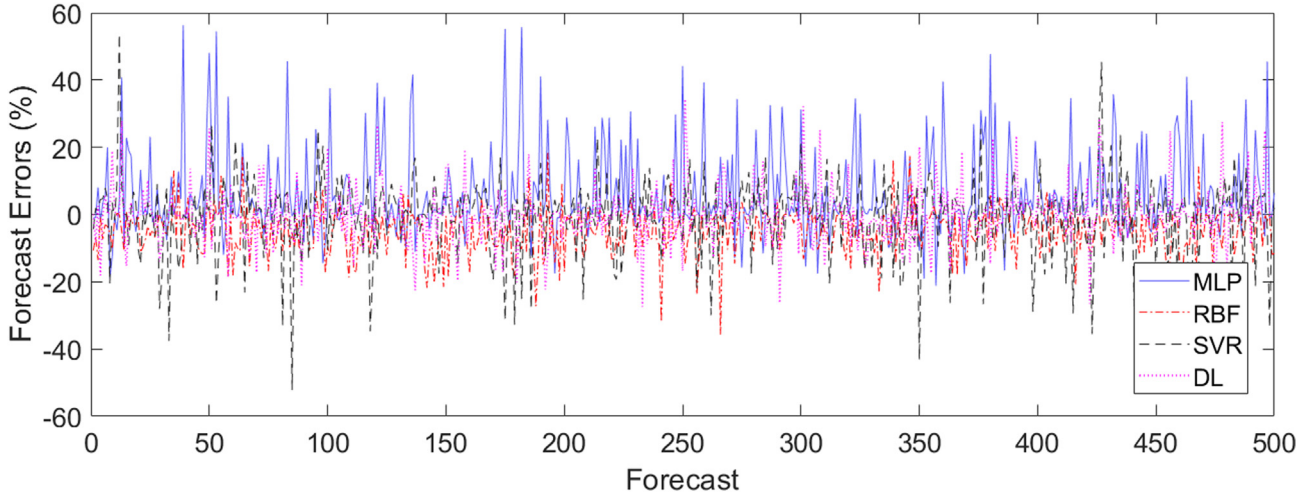


**Fig. 18.** Forecast errors in September 2004, Fortaleza, Brazil.

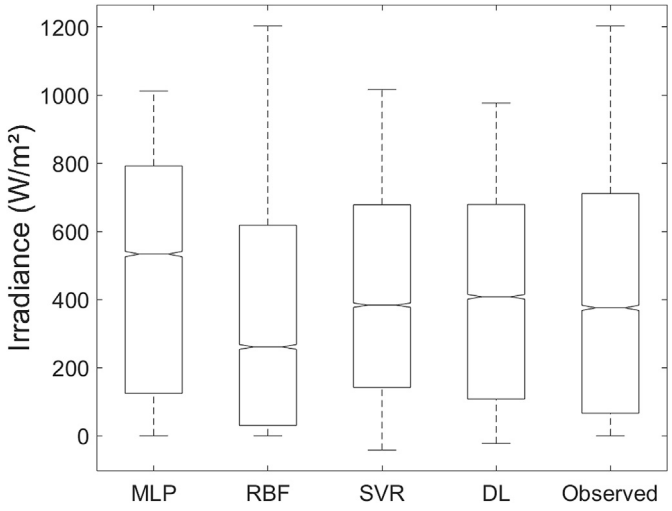


**Fig. 19.** Observed and forecast data boxplot for Fortaleza, Brazil.

$p13$ (75% RBF − 25% SVR). The second layer is defined with connection $p$ 1 (40%− $p11$ 60% $p$ 12) and connection $p$ 2 (50%− $p11$ 50% $p13$). PrevPT output is defined as 75% $p$ 1 and 25% $p$ 2.

Efficient Frontier results show that the optimal portfolio, i. e., the combination with best predictability results, is 10.62% MLP, 70.5% RBF, 3.13% SVR and 15.75% DL. PrevPT, in its characteristic of self-adaptive structure, found the best combination that can be seen in Fig. 23 (a) in its complete structure and (b) in its simplified form mathematically.

The comparison between the distribution of prediction errors is shown in Fig. 24.

For PrevPT, 73.62% of the forecasts underestimate solar energy availability and 26.37% overestimate solar resource. The highest negative error is −30.64%, while the highest positive one is 24.69%. 90.23% of the predictions show forecasting errors between −10% and 10%. Average forecasting error is −3.05% and MAPE for this ANN is 4.52%, which defines integration methodology as an improvement of individual AI results, since MLP MAPE is 8.53%, RBF MAPE is 6.32%, SVR MAPE is 8% and DL MAPE is 6.08%. Table 4 compares individual AI results, partial and final integrations made by PrevPT for the Brazilian data. The comparison uses the same database, horizons and forecast period, in order to generate a SE of the forecasting techniques.

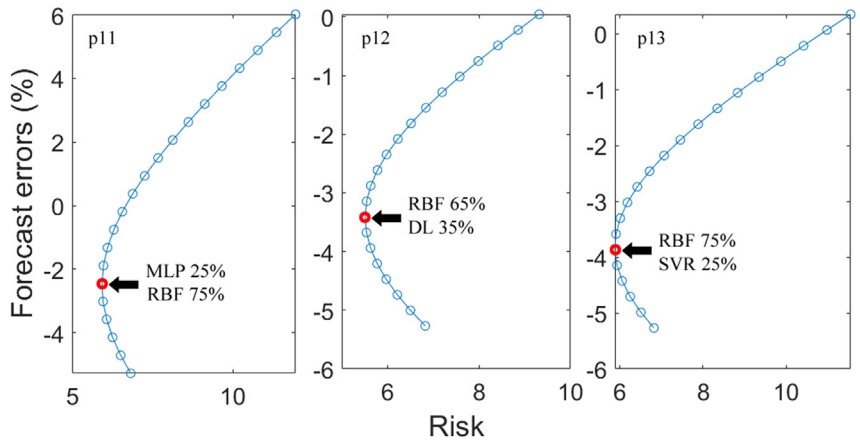


**Fig. 20.** Developed efficient frontiers (first layer).

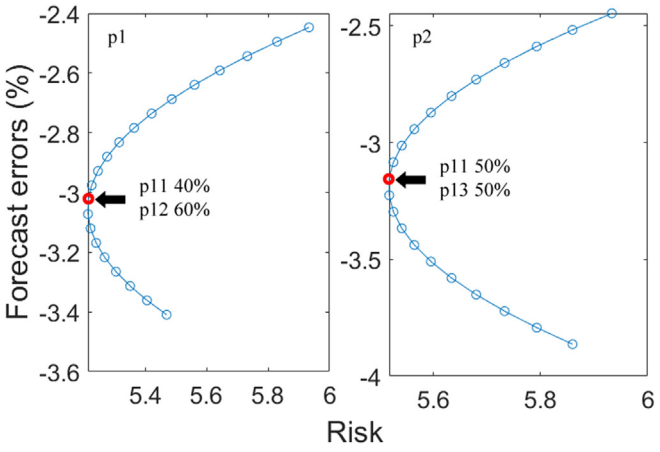


**Fig. 21.** Developed efficient frontiers (second layer).

In the city of Fortaleza, the climate can be divided into rainy and rainless sessions. For this reason, the data collected for these two sessions were separated during the test period to prove the applicability of the techniques used under different climatic conditions. Table 5 compares the MAPEs values obtained for both sessions. MAPEs values of the different (AIs and PrevPT) are very similar for the rainy and rainless sessions.

Fig. 25 presents the Boxplot of the forecasting techniques for both situations. The results show that the behavior of the techniques is very similar for both sessions with different solar availability. This characteristic can be observed comparing the DL interquartile range limits: 3.69%–2.75% for rainy season and −3.62%–3.47% for rainless session.

### 3.6. Discussions

As demonstrated by the MAPE, the techniques obtained satisfactory results regarding the solar resource forecast. Characteristics such as higher variance and standard deviation may justify worse prediction indexes obtained in Spain by almost all techniques. The worst performance was obtained by SVR, with MAPE of 8.34% in the case of Spain and MAPE of 8% in the case of Brazil, which can be defined as good, considering that these techniques obtained an average hit rate of 91.66% and 92%, respectively.

DL used for forecasting stands out in comparison to all the individual forecast techniques (MLP, RBF and SVR). Hence, the use of DL as solar resource predictor is highly beneficial for the expansion of PV power; the implementation of this technique allows for significant improvements over the other techniques used for comparison.

Considering the use of PrevPT for the integration of forecasting techniques, the methodology managed to find an ideal weighting for the impact of each of the individual prediction techniques, as well as in its adaptive structure, was able to disregard some technique which may be causing negative impacts to a solar resource

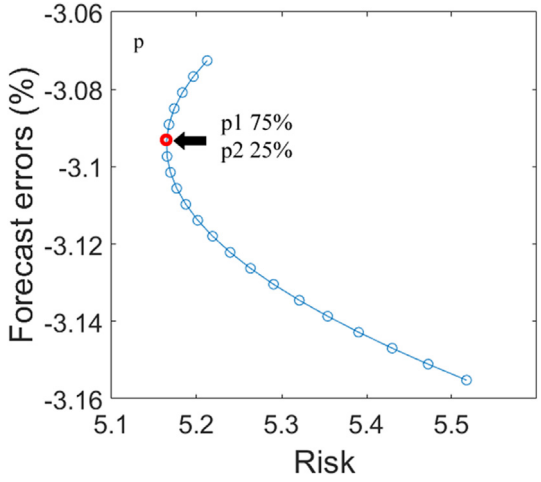


**Fig. 22.** Developed efficient frontiers (output).

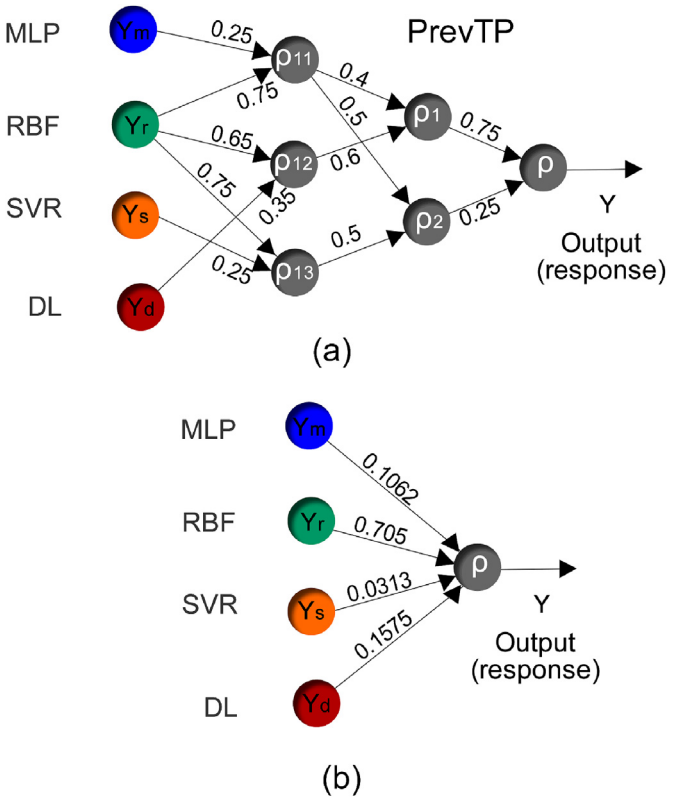


**Fig. 23.** Final weights and structure PrevPT Brazil.

**Table 4**
Comparison of the forecasting results for Brazilian data.

| | MAPE (%) | MPE (%) | Range −10 (%) to 10 (%) |
|---|---|---|---|
| MLP | 8.53 | 6.01 | 70.48 |
| RBF | 6.32 | −5.27 | 75.73 |
| SVR | 8 | 0.35 | 72.32 |
| DL | 6.08 | 0.06 | 78.68 |
| MLP/RBF | 4.82 | −2.45 | 88.8 |
| MLP/SVR | 6.57 | 3.18 | 77.71 |
| RBF/SVR | 5.3 | −3.86 | 85.82 |
| MLP/RBF/SVR | 5.06 | −3.28 | 84.65 |
| MLP/RBF/SVR/DL | 4.52 | −3.05 | 90.23 |

**Table 5**
MAPE for the rainy and rainless season in Brazil.

| | Rainless session | Rainy season |
|---|---|---|
| MLP | 8.52% | 8.77% |
| RBF | 6.32% | 6.16% |
| SVR | 8.01% | 7.71% |
| DL | 6.09% | 5.59% |
| PrevPT | 4.52% | 4.51% |

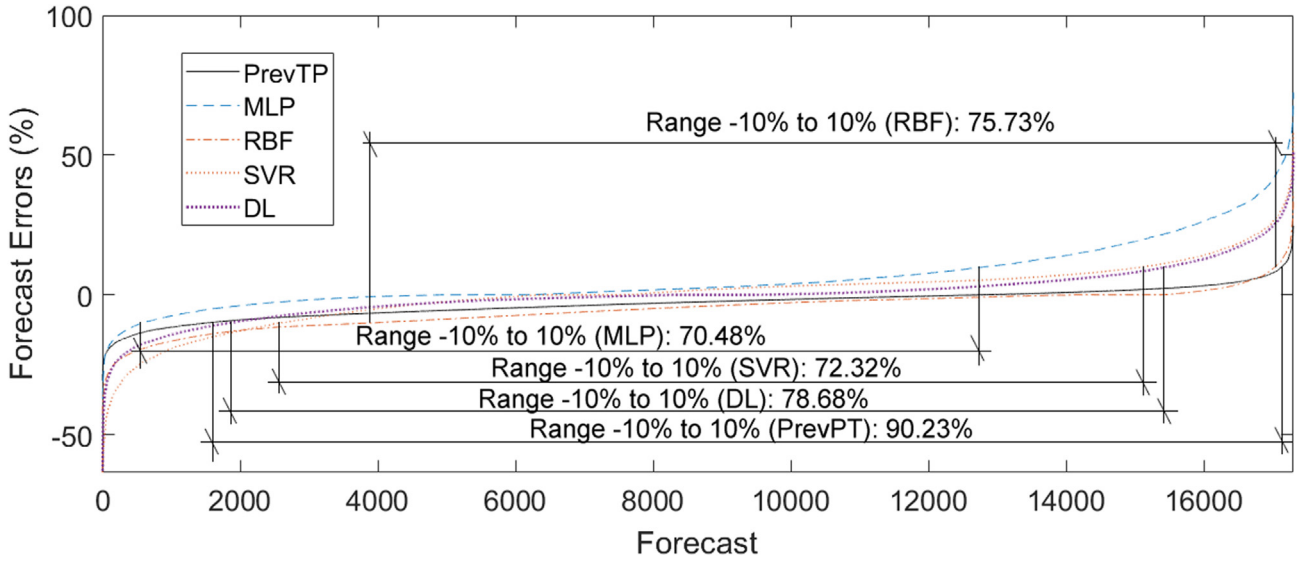


**Fig. 24.** Forecasting error distributions for the data from Brazil.

forecasting system. PrevPT, in its final integration and almost all partial integrations, obtained the best indices in the evaluation criteria than the other predictive methods, with final MAPE of 5.36% in the case of Spain and with MAPE of 4.52% in the case of Brazil.

The techniques obtained an average hit rate of 91.66%–95,48%, highlighting the very high quality of the techniques and methods employed.

## 4. Conclusions

DL used for solar prediction obtained better results than the MLP, RBF and SVR techniques. Regarding PrevPT, errors resulting from the integration of forecast techniques had a better performance than the individual errors of each asset. To compare:

- MAPE for MLP, RBF, SVR and DL in Spain was 8.06%, 7.16%, 8.34% and 6.89%, respectively; as for PrevPT, it was 5.36%. In Brazil, MAPE for MLP, RBF, SVR and DL was 8.53%, 6.32%, 8% and 6.08%, respectively; for PrevPT was 4.52%;
- The range −10%–10% for MLP, RBF, SVR and DL in Spain was 71.29%, 73.27%, 73.71% and 75.87%, respectively; for PrevPT, it was 83.42%. In Brazil, the range −10%–10% for MLP, RBF, SVR and DL was 70.48%, 75.73%, 72.32% and 78.68%, respectively; for PrevPT was 90.23%;

Hence, the use of DL as a solar resource predictor has a significant gain in relation to other individual forecasting methods.

The use of PrevPT is proposed as a methodology to find ideal impacts of AIs. The proposed PrevPT is able to establish the integration of four distinct AI forecasting methods, thus determining an optimal participation of each prediction technique, aiming to reduce predictability errors. It can be concluded that PrevPT is a tool with significant positive impacts for better solar energy management, which can be subjected to different climatic conditions, with different solar resource availability and different locations, as presented and tested herein.

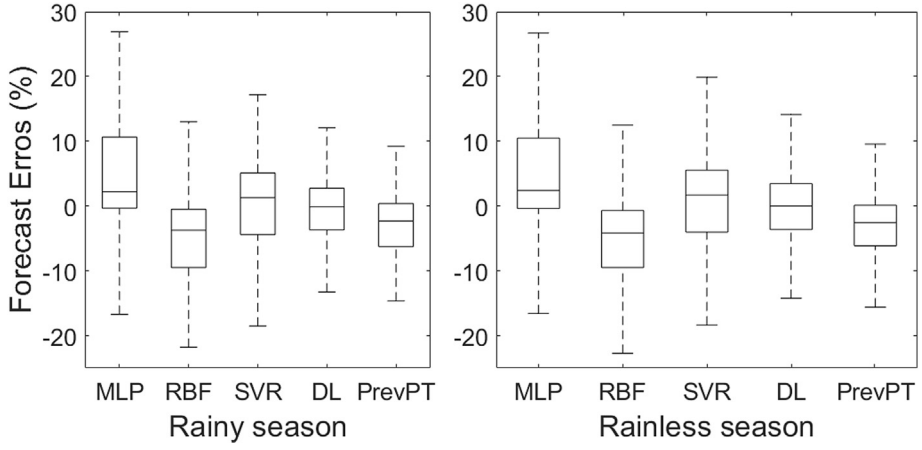


**Fig. 25.** Boxplot for the rainy and rainless season in Brazil.

## Acknowledgement

The authors would like to thank the Coordination for Higher Education Staff Development (CAPES) and the National Council for Scientific and Technological Development (CNPq) for the sandwich doctorate scholarship awarded to the first author; CNPq for researcher scholarship awarded to the second author; PVGIS of the European Commission/IET, for Irradiance and ambient temperature data from Spain; and the Federal University of Ceará for Irradiance and ambient temperature data from Brazil.

## References

[1] Alessandrini S, Delle ML, Sperati S, Cervone G. An analog ensemble for short-term probabilistic solar power forecast. Appl Energy 2015;157:95–110. https://doi.org/10.1016/j.apenergy.2015.08.011.
[2] Elsinga B, Sark Wgjhmv. Short-term peer-to-peer solar forecasting in a network of photovoltaic systems. Appl Energy 2017;206:1464–83. https://doi.org/10.1016/j.apenergy.2017.09.115.
[3] Voyant C, Notton G, Kalogirou S, Nivet ML, Paoli C, Motte F, et al. Machine learning methods for solar radiation forecasting: a review. Renew Energy 2017;105:569–82. https://doi.org/10.1016/j.renene.2016.12.095.
[4] Lima MAFB, Carvalho PCM, Carneiro TC, Leite JR, Neto LJB, Rodrigues GKL, et al. Portfolio theory applied to solar and wind resources forecast. IET Renew Power Gener 2017;11:973–8. https://doi.org/10.1049/iet-rpg.2017.0006.
[5] Qing X, Niu Y. Hourly day-ahead solar irradiance prediction using weather forecasts by LSTM. Energy 2018;148:461–8. https://doi.org/10.1016/j.energy.2018.01.177.
[6] Nam SB, Hur J. A hybrid spatio-temporal forecasting of solar generating resources for grid integration. Energy 2019;177:503–10. https://doi.org/10.1016/j.energy.2019.04.127.
[7] Yagli GM, Yang D, Srinivasan D. Reconciling solar forecasts: sequential reconciliation. Sol Energy 2019;179:391–7. https://doi.org/10.1016/j.solener.2018.12.075.
[8] Yang D. A universal benchmarking method for probabilistic solar irradiance forecasting. Sol Energy 2019;184:410–6. https://doi.org/10.1016/j.solener.2019.04.018.
[9] Trapero JR, Kourentzes N, Martin A. Short-term solar irradiation forecasting based on dynamic harmonic regression. Energy 2015;84:289–95. https://doi.org/10.1016/j.energy.2015.02.100.
[10] Croonenbroeck C, Stadtmann G. Renewable generation forecast studies – review and good practice guidance. Renew Sustain Energy Rev 2019;108:312–22. https://doi.org/10.1016/j.rser.2019.03.029.
[11] Gigoni L, Betti A, Crisostomi E, Franco A, Tucci M, Bizzarri F, et al. Day-Ahead hourly forecasting of power generation from photovoltaic plants. IEEE Trans Sustain Energy 2018;9:831–42. https://doi.org/10.1109/TSTE.2017.2762435.
[12] Bedi J, Toshniwal D. Deep learning framework to forecast electricity demand. Appl Energy 2019;238:1312–26. https://doi.org/10.1016/j.apenergy.2019.01.113.
[13] Chou JS, Ngo NT, Chong WK. The use of artificial intelligence combiners for modeling steel pitting risk and corrosion rate. Eng Appl Artif Intell 2017;65:471–83. https://doi.org/10.1016/j.engappai.2016.09.008.
[14] Camelo HN, Lucio PS, Junior JBVL, Carvalho PCM, Santos DVG. Innovative hybrid models for forecasting time series applied in wind generation based on the combination of time series models with artificial neural networks. Energy 2018;151:347–57. https://doi.org/10.1016/j.energy.2018.03.077.
[15] Monjoly S, André M, Calif R, Soubdhan T. Hourly forecasting of Global Solar Radiation based on a multiscale decomposition method: a hybrid approach. Energy 2017;119:288–98. https://doi.org/10.1016/j.energy.2016.11.061.
[16] Calif R, Schmitt F, Huang Y, Soubdhan T. Intermittency study of high frequency global solar radiation sequences under a tropical climate. Sol Energy 2013;98:349–65. https://doi.org/10.1016/j.solener.2013.09.018.
[17] Das UK, Tey KS, Seyedmahmoudian M, Mekhilef S, Idris MYI, Deventer WV, et al. Forecasting of photovoltaic power generation and model optimization: a review. Renew Sustain Energy Rev 2018;81:912–28. https://doi.org/10.1016/j.rser.2017.08.017.
[18] Mellit A, Pavan AM. A 24-h forecast of solar irradiance using artificial neural network: application for performance prediction of a grid-connected PV plant at Trieste, Italy. Sol Energy 2010;84:807–21. https://doi.org/10.1016/j.solener.2010.02.006.
[19] Alfadda A, Rahman S, Pipattanasomporn M. Solar irradiance forecast using aerosols measurements: a data driven approach. Sol Energy 2018;170:924–39. https://doi.org/10.1016/j.solener.2018.05.089.
[20] Chu Y, Li M, Coimbra CFM. Sun-tracking imaging system for intra-hour DNI forecasts. Renew Energy 2016;96:792–9. https://doi.org/10.1016/j.renene.2016.05.041.
[21] Jiang H, Dong Y, Wang J, Li Y. Intelligent optimization models based on hard-ridge penalty and RBF for forecasting global solar radiation. Energy Convers Manag 2015;95:42–58. https://doi.org/10.1016/j.enconman.2015.02.020.
[22] Awad M, Qasrawi I. Enhanced RBF neural network model for time series prediction of solar cells panel depending on climate conditions (temperature and irradiance). Neural Comput Appl 2016;30:1757–68. https://doi.org/10.1007/s00521-016-2779-5.
[23] Haykin S. Redes Neurais: princípios e prática. 2th ed. Porto Alegre: Bookman; 2001.
[24] Belaid S, Mellit A. Prediction of daily and mean monthly global solar radiation using support vector machine in an arid climate. Energy Convers Manag 2016;118:105–18. https://doi.org/10.1016/j.enconman.2016.03.082.
[25] Zeng J, Qiao W. Short-term solar power prediction using a support vector machine. Renew Energy 2013;52:118–27. https://doi.org/10.1016/j.renene.2012.10.009.
[26] Meenal R, Selvakumar AI. Assessment of SVM, empirical and ANN based solar radiation prediction models with most influencing input parameters. Renew Energy 2018;121:324–43. https://doi.org/10.1016/j.renene.2017.12.005.
[27] Moncada A, Richardson W, Vega-Avila R. Deep learning to forecast solar irradiance using a six-month UTSA SkyImager dataset. Energies 2018;11:1988. https://doi.org/10.3390/en11081988.
[28] Kaba K, Sarıgül M, Avcı M, Kandırmaz HM. Estimation of daily global solar radiation using deep learning model. Energy 2018;162:126–35. https://doi.org/10.1016/j.energy.2018.07.202.
[29] Brusaferri A, Matteucci M, Portolani P, Vitali A. Bayesian deep learning based method for probabilistic forecast of day-ahead electricity prices. Appl Energy 2019;250:1158–75. https://doi.org/10.1016/j.apenergy.2019.05.068.
[30] Sun Y, Venugopal V, Brandt AR. Short-term solar power prediction with deep learning : exploring optimal input and output configuration. Sol Energy 2019;188:730–41. https://doi.org/10.1016/j.solener.2019.06.041.
[31] Ahmad T, Chen H. Deep learning for multi-scale smart energy forecasting. Energy 2019;98–112. https://doi.org/10.1016/j.energy.2019.03.080.
[32] Speth V. Diversification of wind and solar energy portfolio risk an explorative analysis for Germany 2010-2012. University of St. Gallen; 2013.
[33] Shahriari M, Blumsack S. The capacity value of optimal wind and solar portfolios. Energy 2018;148:992–1005. https://doi.org/10.1016/j.energy.2017.12.121.
[34] Santos-Alamillos FJ, Thomaidis NS, Usaola-García J, Ruiz-Arias JA, Pozo-Vázquez D. Exploring the mean-variance portfolio optimization approach for planning wind repowering actions in Spain. Renew Energy 2017;106:335–42. https://doi.org/10.1016/j.renene.2017.01.041.
[35] Narayan A, Ponnambalam K. Risk-averse stochastic programming approach for microgrid planning under uncertainty. Renew Energy 2017;101:399–408. https://doi.org/10.1016/j.renene.2016.08.064.
[36] Tola M. Applying modern portfolio theory to plant electricity planning in Albania. Eur Sci J 2015;11:247–52.
[37] ShahNazari M, Maybee B, Whale J, McHugh A. Climate policy uncertainty and power generation investments: a real options-CVaR portfolio optimization approach. Energy Procedia 2015;75:2649–57. https://doi.org/10.1016/j.egypro.2015.07.367.
[38] Cunha J, Ferreira PV. Designing electricity generation portfolios using the mean-variance approach. Int J Sustain Energy Plan Manag 2014;4:17–30. https://doi.org/10.5278/ijsepm.2014.4.3.
[39] Bishop CM. Pattern Recognition and Machine Learning. first ed. New York: Springer; 2006.
[40] Calsing LC. Previsão de demanda combinada a partir de métodos quantitativos e opinião de especialistas. Federal University of Rio Grande do Sul; 2015.
[41] Qiu X, Zhang L, Ren Y, Suganthan P, Amaratunga G. Ensemble deep learning for regression and time series forecasting. IEEE Symp. Ser. Comput. Intell. - CIEL 2014 2014 IEEE Symp. Comput. Intell. Ensemble learn. Proc. IEEE; 2014. p. 1–6. https://doi.org/10.1109/CIEL.2014.7015739. IEEE SSCI, 2014 - 2014.
[42] Hochreiter S, Schmidhuber J. Long short-term memory. Neural Comput 1997;9:1735–80. https://doi.org/10.1162/neco.1997.9.8.1735.
[43] Wang W, Hong T, Xu X, Chen J, Liu Z, Xu N. Forecasting district-scale energy dynamics through integrating building network and long short-term memory learning algorithm. Appl Energy 2019;248:217–30. https://doi.org/10.1016/j.apenergy.2019.04.085.